24. C. J. Evans *et al.*, *Astrophys. J.* **715**, L74 (2010).
25. O. Schnurr, A. F. J. Moffat, A. Villar-Sbaffi, N. St-Louis, N. I. Morrell, *Mon. Not. R. Astron. Soc.* **395**, 823 (2009).
26. But see (*30*), according to whom M_b = 240 $M_\odot$.
27. See http://acis.mit.edu/acis.
28. L. K. Townsley, P. S. Broos, E. D. Feigelson, G. P. Garmire, K. V. Getman, *Astron. J.* **131**, 2164 (2006).
29. K. A. van der Hucht *et al.*, in *Massive Stars in Interactive Binaries*, N. St.-Louis, A. F. J. Moffat, Eds., vol. 367 of *Astronomical Society of the Pacific Conference Series* (Astronomical Society of the Pacific, 2007), p. 159.
30. A.-N. Chené, O. Schnurr, P. A. Crowther, E. Fernández-Lajús, A. F. J. Moffat, in *IAU Symposium*, C. Neiner, G. Wade, G. Meynet, G. Peters, Eds., vol. 272 of *IAU Symposium* (International Astronomical Union, 2011), p. 497.
31. S. Portegies Zwart, E. Gaburov, H.-C. Chen, M. A. Gürkan, *Mon. Not. R. Astron. Soc.* **378**, L29 (2007).
32. M. Fujii, M. Iwasawa, Y. Funato, J. Makino, *Astrophys. J.* **686**, 1082 (2008).
33. P. Massey, L. R. Penny, J. Vukovich, *Astrophys. J.* **565**, 982 (2002).
34. O. Schnurr, J. Casoli, A.-N. Chen'e, A. F. J. Moffat, N. St-Louis, *Mon. Not. R. Astron. Soc.* **389**, L38 (2008).
35. W. D. Taylor *et al.*, *Astron. Astrophys.* **530**, L10 (2011).
36. A. F. J. Moffat, in *IAU Symposium*, F. Bresolin, P. A. Crowther, J. Puls, Eds., vol. 250 of *IAU Symposium* (International Astronomical Union, 2008), p. 119.
37. E. Koumpia, A. Z. Bonanos, http://arxiv.org/abs/1009.4709 (2010).
38. A. E. Piatti, E. Bica, J. J. Claria, *Astron. Astrophys. Suppl Ser.* **127**, 423 (1998).

Acknowledgments: We thank B. Brandl, A. Brown, A. Gürkan, K. Nitadori, and H. Sana for discussions and the anonymous referees for their constructive criticism. This work was supported by Research Fellowships of the Japan Society for the Promotion of Science for Young Scientists and the Netherlands Research Council NWO [grants VICI (639.073.803), AMUSE (614.061.608), and Little Green Machine] and by the Netherlands Research School for Astronomy. The simulation software is available at http://amusecode.org and the data can be found at http://initialconditions.org.

A Perovskite Oxide Optimized for Oxygen Evolution Catalysis from Molecular Orbital Principles

Jin Suntivich,[1,2] Kevin J. May,[2,3] Hubert A. Gasteiger,[2,3]* John B. Goodenough,[4] Yang Shao-Horn[1,2,3]†

The efficiency of many energy storage technologies, such as rechargeable metal-air batteries and hydrogen production from water splitting, is limited by the slow kinetics of the oxygen evolution reaction (OER). We found that $Ba_{0.5}Sr_{0.5}Co_{0.8}Fe_{0.2}O_{3-\delta}$ (BSCF) catalyzes the OER with intrinsic activity that is at least an order of magnitude higher than that of the state-of-the-art iridium oxide catalyst in alkaline media. The high activity of BSCF was predicted from a design principle established by systematic examination of more than 10 transition metal oxides, which showed that the intrinsic OER activity exhibits a volcano-shaped dependence on the occupancy of the 3d electron with an e_g symmetry of surface transition metal cations in an oxide. The peak OER activity was predicted to be at an e_g occupancy close to unity, with high covalency of transition metal–oxygen bonds.

The design of cost-effective, highly active catalysts for energy storage applications is a critical element in the societal pursuit of sustainable energy. The oxygen evolution reaction (OER) in particular is an enabling process for many energy storage options, such as direct-solar (*1, 2*) and electricity-driven (*3*) water splitting ($H_2O \rightarrow H_2 + \frac{1}{2}O_2$) and rechargeable metal-air batteries ($M_xO_2 \rightarrow M_x + O_2$) (*4, 5*). However, the kinetics of the OER are sluggish, even when facilitated by comparatively high-activity, precious metal–containing catalysts. This limitation imposes a considerable overpotential requirement (*6, 7*), similar to the case of the oxygen reduction reaction (ORR) (*8, 9*) for fuel cell applications (*10*). First-row transition metal oxides such as $NiCo_2O_4$ (*11*) and $LaNiO_3$ (*12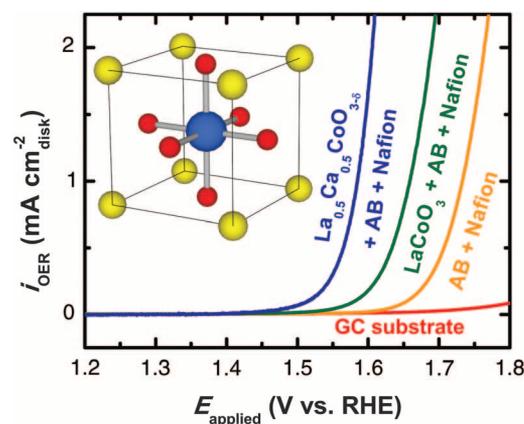*) are cost-effective alternatives, but they underperform relative to iridium oxide (IrO_2), which is considered to be state of the art (table S1). As part of efforts to discover highly active catalysts based on abundant elements, substantial effort has been devoted to understanding the mechanism and parameters that govern the OER activity and ideally discovering a convenient activity descriptor. Trasatti (*13*), Bockris and Otagawa (*12*), and Rossmeisl *et al.* (*7, 14*) have reported the enthalpy of a lower to higher oxide transition, the 3d electron number of bulk transition metal ions, and the surface oxygen binding energy as OER activity descriptors, respectively. However, it is not straightforward to predict transition metal oxides with high OER activity by means of these proposed descriptors (*7, 12, 13*).

Motivated by the success of the d-band theory as the activity descriptor for metal surfaces (*15*), we seek a simple activity descriptor that will accomplish a similar correlation between surface adsorbate binding and catalytic activity for transition metal oxides. Here we report a distinct OER activity design principle, namely that a near-unity occupancy of the e_g orbital of surface transition metal ions and high covalency in bonding to oxygen can enhance the intrinsic OER activity of perovskite transition metal oxides in alkaline solution ($4OH^- \rightarrow O_2 + 2H_2O + 4e^-$). We further show that this design principle has predictive power, from which we were able to identify a highly active OER oxide catalyst.

Our approach is based on a molecular orbital bonding framework. Because the e_g orbital of surface transition metal ions participates in σ-bonding with a surface-anion adsorbate (*16, 17*), its occupancy can greatly influence the binding of oxygen-related intermediate species on B-sites (scheme S1) and thus the OER activity. We elected to study the perovskite structure (Fig. 1, inset) $A_{1-x}A'_xB_yB'_{1-y}O_3$, where A or A' is a rare-earth or alkaline-earth metal and B or B' is a transition metal, because of its flexibility in both physical-chemical and catalytic properties. Representative OER currents of oxides collected in this study (Fig. 1) were obtained by using a thin-film rotating-disk electrode with well-defined oxygen

Fig. 1. Exemplary OER currents of $La_{1-x}Ca_xCoO_3$ and $LaCoO_3$ thin films on GCE in O_2-saturated 0.1 M KOH at 10 mV s^{-1} scan rate at 1600 rpm, capacitance-corrected by taking an average of the positive and negative scans. The contributions from AB and binder (Nafion) in the thin film and GCE are shown for comparison. The inset shows the structure of perovskite ABO_3 (where A is an alkali or a rare earth, yellow; B is a transition metal, blue; and O is oxygen, red).

[1]Materials Science and Engineering Department, Massachusetts Institute of Technology, Cambridge, MA 02139, USA. [2]Electrochemical Energy Laboratory, Massachusetts Institute of Technology, Cambridge, MA 02139, USA. [3]Mechanical Engineering Department, Massachusetts Institute of Technology, Cambridge, MA 02139, USA. [4]Texas Materials Institute, University of Texas, Austin, TX 78712, USA.

*Present address: Department of Chemistry, Technische Universität München, Lichtenbergstrasse 4, D-85747 Garching, Germany.

†To whom correspondence should be addressed. E-mail: shaohorn@mit.edu

transport (*18*). The background contributions for OER from a carbon additive (acetylene black, AB) and Nafion in the oxide films and GCE (glassy carbon electrode) are negligible below ~1.65 V versus RHE (reversible hydrogen electrode) (Fig. 1).

To separate the surface area effect from the intrinsic catalytic activity, we analyzed the surface area–normalized kinetic current density (referred to as specific activity, i_s) as a function of voltage versus RHE to assess the intrinsic OER activities of the perovskite oxides (fig. S1). Our measurements consistently yielded a comparable or higher specific OER activity of oxides than those found in previous reports (*12*, *19–22*) (table S2). This discrepancy can be attributed to a higher catalyst utilization in thin films (<10 cm^2_{ox}/cm^2_{disk}) on GCE (*18*, *23*) than on traditional porous electrodes used in earlier work, which have a very high internal surface area (~10^4 cm^2_{ox}/cm^2_{disk}) and so yield less accurate determinations of the specific activity of powder oxide catalysts.

Our studies showed that the specific OER activities of the perovskite oxides exhibit a volcano shape as a function of the e_g filling of surface B-site cations (Fig. 2), where the activities are compared in terms of the overpotential required to provide a specific current of 50 $\mu A/cm^2_{ox}$. In this analysis, the e_g filling of B-site ions was estimated from a combination of literature data and results of thermogravimetry and x-ray absorption studies (*24*); partial substitution on the A- or B-sites, resulting in oxygen vacancy or B-site ion valence changes, was taken into consideration. The assignment of the e_g-orbital occupancy for oxides with two different B-site ions such as $LaMn_{0.5}Cu_{0.5}O_3$ was based on the more active surface transition metal cation under an assumption that the less active cation contributes negligibly. With a Tafel slope of ~60 mV/decade, the e_g occupancy correlated with the specific OER activities of oxides across four orders of magnitude, over a voltage span of 0.3 V; this observation allows identification of e_g filling of surface transition metal cations as a universal activity descriptor for these oxides.

The e_g-filling descriptor proposed in this study is fundamentally different from the number of 3d electrons (both e_g and t_{2g} electrons) of bulk B-site cations proposed by Otagawa and Bockris (*12*) or the conduction band described by Matsumoto (*20*). The filling of the surface transition metal antibonding states of e_g-orbital parentage is a more appropriate descriptor for catalysis because the σ-bonding e_g orbital has a stronger overlap with the oxygen-related adsorbate than does the π-bonding t_{2g} orbital, and thus can more directly promote electron transfer between surface cation and adsorbed reaction intermediates. Moreover, lowering of the site symmetry at the surface can induce orbital localization and modify the surface electronic state to differ from that of the bulk (*25*), and the use of the surface e_g filling as opposed to the bulk value is crucial to prescribe accurately the catalytic trend for ORR on oxides (*26*). Our observation of the importance of the surface

spin state in the O₂ electrocatalysis may help to explain the difference between the trend of OER activity of perovskites in this study and that of previous ab initio work (*14*) (as the trend in the binding energy with oxygenated species on B-site ions would be expected to be different as well).

We explain the OER activity trend in Fig. 2 as follows. Considering the ab initio finding of Rossmeisl *et al.* (*7*), whose work suggests a universal dependence of the OER activity on the oxygen binding strength, we propose that the e_g filling of surface transition metal cations can greatly influence the binding of OER intermediates to the oxide surface and thus the OER activity. For the right branch of the volcano, the rate-determining step (RDS) is the formation of the O-O bond in OOH adsorbate on B-site ions ($B^{(m+1)+}-O^{2-} + OH^- \rightarrow B^{(m)+}-OOH^- + e^-$), whereas for the left

branch of the volcano, the deprotonation of the oxyhydroxide group to form peroxide ions ($B^{(m)+}-OOH^- + OH^- \rightarrow B^{(m+1)+}-O_2^{2-} + H_2O + e^-$) may be rate-limiting (scheme S2) (*7*). Having e_g filling close to unity experimentally facilitates these RDSs efficiently and thereby leads to the highest OER activity. Our molecular orbital model is further supported by the observation that the OER activity can be enhanced with increasing covalent mixing between B-site ion and O atoms of oxides at a constant e_g filling (fig. S2), where an active redox couple lies at the top of the O-2p bands. Greater covalency between B-site and oxygen, where the active redox couple of the B-site ion has a larger O-2p character, promotes the charge transfer between surface cations and adsorbates such as O_2^{2-} and O^{2-} in the RDSs of OER, which can result in higher OER activity.

Fig. 2. The relation between the OER catalytic activity, defined by the overpotentials at 50 μA cm^{-2}_{ox} of OER current, and the occupancy of the e_g-symmetry electron of the transition metal (B in ABO_3). Data symbols vary with type of B ions (Cr, red; Mn, orange; Fe, beige; Co, green; Ni, blue; mixed compounds, purple), where $x = 0$, 0.25, and 0.5 for Fe. Error bars represent SDs of at least three independent measurements. The dashed volcano lines are shown for guidance only.
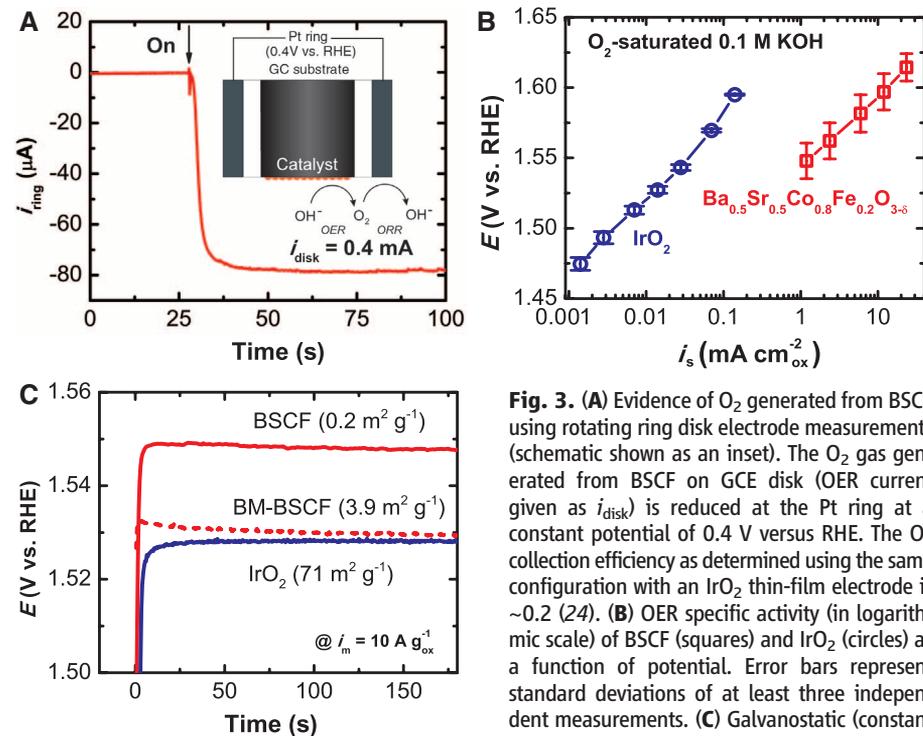
Fig. 3. (**A**) Evidence of O₂ generated from BSCF using rotating ring disk electrode measurements (schematic shown as an inset). The O₂ gas generated from BSCF on GCE disk (OER current given as i_{disk}) is reduced at the Pt ring at a constant potential of 0.4 V versus RHE. The O₂ collection efficiency as determined using the same configuration with an IrO_2 thin-film electrode is ~0.2 (*24*). (**B**) OER specific activity (in logarithmic scale) of BSCF (squares) and IrO_2 (circles) as a function of potential. Error bars represent standard deviations of at least three independent measurements. (**C**) Galvanostatic (constant current) measurement of mass activities of BSCF, BM-BSCF, and IrO_2.

The OER design principle shown in Fig. 2 was applied to obtain a highly active OER catalyst, BSCF, which was best known for its high performance as a cathode in solid oxide fuel cells (27) and oxygen permeation membranes. Because the surface Co cations of BSCF are in the intermediate spin state (28, 29), the electronic configuration of Co cations (estimated oxidation state of ~2.8; table S3) in BSCF can be assigned as $t_{2g}^5 e_g^{~1.2}$. We found that BSCF (fig. S3) had the highest OER activity among all oxides studied as predicted by the e_g activity descriptor (Fig. 2). To ensure that the observed oxidation current was from oxygen evolution, we used a rotating Pt ring electrode held at the ORR potential of 0.4 V versus RHE to detect O_2 gas generated at the catalyst by electrochemical reduction (Fig. 3A). The reduction current detected on the ring electrode suggested that the oxidation current from BSCF could be accounted for fully by the OER. The measured intrinsic OER activity of BSCF was higher than that of IrO_2 nanoparticles (average diameter ~6 nm) (Fig. 3B) by at least an order of magnitude when considering a conservative experimental uncertainty in the intrinsic OER activity of approximately an order of magnitude (24). The exceptional OER activity of BSCF was further confirmed by galvanostatic measurements, which manifested no degradation in the OER activity (fig. S4). Once the sizes of BSCF particles were reduced to submicrometer range via ball-milling, the mass activity of ball-milled BSCF (BM-BSCF) was found to compare favorably with IrO_2, and the overpotential of BM-BSCF was shown to be nearly identical to that of IrO_2 at a catalytic activity normalized to the catalyst's mass (i.e., mass activity) of 10 A g_{ox}^{-1} (Fig. 3C). Developing nanostructured BSCF

could further improve its mass activity and thus yield highly efficient OER electrodes.

Our study suggests the importance of developing a transition metal oxide having a surface cation e_g occupancy close to unity and high B-site oxygen covalency for enhancing the OER catalytic activity. This approach is a promising strategy to create bifunctional oxide catalysts and electrodes for the development of efficient, rechargeable metal-air batteries, regenerative fuel cells, and other rechargeable air-based energy storage devices.

References and Notes

1. H. B. Gray, *Nat. Chem.* **1**, 7 (2009).
2. N. S. Lewis, D. G. Nocera, *Proc. Natl. Acad. Sci. U.S.A.* **103**, 15729 (2006).
3. M. W. Kanan, D. G. Nocera, *Science* **321**, 1072 (2008).
4. Y. C. Lu et al., *J. Am. Chem. Soc.* **132**, 12170 (2010).
5. M. Armand, J. M. Tarascon, *Nature* **451**, 652 (2008).
6. M. T. M. Koper, *J. Electroanal. Chem.* **660**, 254 (2011).
7. J. Rossmeisl, Z. W. Qu, H. Zhu, G. J. Kroes, J. K. Norskov, *J. Electroanal. Chem.* **607**, 83 (2007).
8. H. A. Gasteiger, N. M. Marković, *Science* **324**, 48 (2009).
9. V. R. Stamenkovic et al., *Science* **315**, 493 (2007).
10. H. A. Gasteiger, S. S. Kocha, B. Sompalli, F. T. Wagner, *Appl. Catal. B* **56**, 9 (2005).
11. C. R. Davidson, G. Kissel, S. Srinivasan, *J. Electroanal. Chem.* **132**, 129 (1982).
12. J. O. Bockris, T. Otagawa, *J. Electrochem. Soc.* **131**, 290 (1984).
13. S. Trasatti, *J. Electroanal. Chem.* **111**, 125 (1980).
14. I. C. Man et al., *ChemCatChem* **3**, 1159 (2011).
15. B. Hammer, J. K. Nørskov, *Adv. Catal.* **45**, 71 (2000).
16. C. J. Ballhausen, H. B. Gray, *Inorg. Chem.* **1**, 111 (1962).
17. T. A. Betley, Q. Wu, T. Van Voorhis, D. G. Nocera, *Inorg. Chem.* **47**, 1849 (2008).
18. J. Suntivich, H. A. Gasteiger, N. Yabuuchi, Y. Shao-horn, *J. Electrochem. Soc.* **157**, B1263 (2010).
19. Y. Matsumoto, J. Kurimoto, E. Sato, *J. Electroanal. Chem.* **102**, 77 (1979).
20. Y. Matsumoto, H. Manabe, E. Sato, *J. Electrochem. Soc.* **127**, 811 (1980).
21. Y. Matsumoto, E. Sato, *Electrochim. Acta* **24**, 421 (1979).
22. A. Wattiaux, J. C. Grenier, M. Pouchard, P. Hagenmuller, *J. Electrochem. Soc.* **134**, 1714 (1987).
23. T. J. Schmidt et al., *J. Electrochem. Soc.* **145**, 2354 (1998).
24. See supporting material on *Science* Online.
25. J. Q. Yan, J. S. Zhou, J. B. Goodenough, *Phys. Rev. B* **70**, 014402 (2004).
26. J. Suntivich et al., *Nat. Chem.* **3**, 546 (2011).
27. Z. P. Shao, S. M. Haile, *Nature* **431**, 170 (2004).
28. A. S. Harvey et al., *Phys. Chem. Chem. Phys.* **11**, 3090 (2009).
29. A. S. Harvey et al., *J. Phys. Condens. Matter* **21**, 015801 (2009).

Climate Sensitivity Estimated from Temperature Reconstructions of the Last Glacial Maximum

Andreas Schmittner,[1]* Nathan M. Urban,[2] Jeremy D. Shakun,[3] Natalie M. Mahowald,[4] Peter U. Clark,[5] Patrick J. Bartlein,[6] Alan C. Mix,[1] Antoni Rosell-Melé[7]

Assessing the impact of future anthropogenic carbon emissions is currently impeded by uncertainties in our knowledge of equilibrium climate sensitivity to atmospheric carbon dioxide doubling. Previous studies suggest 3 kelvin (K) as the best estimate, 2 to 4.5 K as the 66% probability range, and nonzero probabilities for much higher values, the latter implying a small chance of high-impact climate changes that would be difficult to avoid. Here, combining extensive sea and land surface temperature reconstructions from the Last Glacial Maximum with climate model simulations, we estimate a lower median (2.3 K) and reduced uncertainty (1.7 to 2.6 K as the 66% probability range, which can be widened using alternate assumptions or data subsets). Assuming that paleoclimatic constraints apply to the future, as predicted by our model, these results imply a lower probability of imminent extreme climatic change than previously thought.

Climate sensitivity is the change in global mean near-surface air temperature ΔSAT caused by an arbitrary perturbation ΔF (radiative forcing) of Earth's radiative balance at the top of the atmosphere with respect to a given reference state. The equilibrium climate sensitivity for a doubling of atmospheric carbon dioxide (CO_2) concentrations (ECS_{2xC}) from preindus-

trial times has been established as a well-defined standard measure (1). Moreover, because transient (disequilibrium) climate change and impacts on ecological and social systems typically scale with ECS_{2xC}, it is a useful and important diagnostic in climate modeling (1). Initial estimates of $ECS_{2xC} = 3 \pm 1.5$ K suggested a large uncertainty (2), which has not been reduced in the past 32 years despite considerable efforts (1–10). On the contrary, many recent studies suggest a small possibility of very high (up to 10 K and higher) values for ECS_{2xC} (3–10), implying extreme

[1]College of Oceanic and Atmospheric Sciences, Oregon State University, Corvallis, OR 97331–5503, USA. [2]Woodrow Wilson School of Public and International Affairs, Princeton University, NJ 08544, USA. [3]Department of Earth and Planetary Sciences, Harvard University, Cambridge, MA 02138, USA. [4]Department of Earth and Atmospheric Sciences, Cornell University, Ithaca, NY 14850, USA. [5]Department of Geosciences, Oregon State University, Corvallis, OR 97331, USA. [6]Department of Geography, University of Oregon, Eugene, OR 97403, USA. [7]Institució Catalana de Recerca i Estudis Avançats and Institute of Environmental Science and Technology, Autonomous University of Barcelona, Bellaterra, Spain.

*To whom correspondence should be addressed. E-mail: aschmitt@coas.oregonstate.edu